Acta Cryst. (1975). A31, 1

The Use of a Three-Axis Spectrometer on an Angled Reactor Channel

BY B. C. G. HAYWOOD

A.E.R.E., Harwell, Didcot, Berkshire, England

(*Received* 11 *March* 1974; *accepted* 23 *July* 1974)

The resolution function is derived for a three-axis neutron spectrometer in which the monochromator scattering plane is at an angle to the specimen and analyser scattering planes. The analysis shows that the width of measured peaks is much more affected by the slope of the dispersion surface under investigation than by the angle between the planes. It is concluded that a spectrometer which is used on a hole inclined at 35° would have satisfactory resolution and intensity for most purposes.

Introduction

In an earlier paper (Haywood, 1974), referred to as I, the general problems of the resolution function of a two-axis diffractometer installed on an angled reactor channel were considered. In the present paper, the analysis, again based on Gaussian mosaic and collimation functions, is extended to deal with the case of the three-axis spectrometer.

It is widely believed that the resolution function of a spectrometer in which the scattering planes of monochromator and sample are not parallel is very much inferior to that of a conventional instrument. In this paper it is shown that the measured width of phonon or magnon peaks is much more affected by small changes in the slope of the dispersion curve than by the difference in angle between the monochromator and specimen scattering planes. Thus it is possible to build a perfectly viable three-axis spectrometer for use on an angled channel in which the monochromator produces a horizontal beam of neutrons and the subsequent scattering processes are carried out entirely in the horizontal plane.

Method of calculation

The resolution function for the conventional three-axis spectrometer has been evaluated by several authors, *e.g.*, Collins (1963), Bjerrum Møller & Nielson (1970), Cooper & Nathans (1967) and Chesser & Axe (1973). The calculations in the present case use the method developed by Cooper & Nathans (1967), referred to as CN.

In the unconventional arrangement discussed in this paper a beam of neutrons emerges from the reactor at an angle to the horizontal and is scattered by the monochromator crystal into a horizontal direction. Subsequent scattering processes at the specimen and analyser crystal are carried out entirely in the horizontal plane. The proposed arrangement is shown diagramatically in Fig. 1. In this figure the mutually orthogonal axes have been chosen so that x and y are horizontal and x is perpendicular to the beam of the neutrons which emerge from the reactor at an angle ψ to the horizontal. The collimators C_0 and C_1' have divergences α_0, α_1' and β_0, β_1' in and normal to the monochromator scattering plane respectively. The subsequent collimators C_1, C_2 and C_3 have horizontal and vertical divergences α_n and β_n respectively.

The associated diagram in reciprocal space is shown in Fig. 2. Neutrons with most probable wave vector $\mathbf{k}_0$ strike the monochromator and are scattered through $2\theta_M$ into the horizontal plane. Neutrons in the beam from the monochromator with most probable wave vector $\mathbf{k}_I$ strike the specimen, are scattered through $2\theta_s$ and change energy. The beam with most probable wave vector $\mathbf{k}_F$ is scattered at the analyser through $2\theta_A$ into the detector. Fig. 2 is Fig. 3 of CN with the first scattering plane rotated through an angle φ about $\mathbf{k}_I$. The value of φ is equal to Ψ only when $\theta_M = 45°$; it can easily be shown that $\sin \Psi = \sin \varphi \sin 2\theta$. This relationship is discussed further in I.

We define $\mathbf{Q}$ as $\mathbf{k}_F - \mathbf{k}_I$. $\mathbf{k}_0, \mathbf{k}_i$, and $\mathbf{k}_f$ are wave vectors corresponding to a particular scattering process and $\Delta\mathbf{k}_i = \mathbf{k}_i - \mathbf{k}_I$, $\Delta\mathbf{k}_f = \mathbf{k}_f - \mathbf{k}_F$, $\Delta\mathbf{Q} = \mathbf{k}_f - \mathbf{k}_i - \mathbf{Q}$. The probability of a neutron being transmitted through the system from source to detector can be shown to be (CN)

$$
\begin{aligned}
&P(\Delta\mathbf{k}_i, \Delta\mathbf{k}_f, \gamma_1, \gamma_1', \gamma_2, \delta_1, \delta_1', \delta_2) \\
&\propto \exp -\tfrac{1}{2}\left[\frac{[(\Delta\mathbf{k}_i/\mathbf{k}_I)\tan\theta_M + \gamma_1]^2}{\eta_M^2}\right. \\
&+ \frac{[(\Delta\mathbf{k}_f/\mathbf{k}_F)\tan\theta_A - \gamma_2]^2}{\eta_A^2} \\
&+ \frac{[2(\Delta\mathbf{k}_i/\mathbf{k}_I)\tan\theta_M + \gamma_1]^2}{\alpha_0^2} \\
&+ \frac{\gamma_1^2}{\alpha_1^2} + \frac{[2(\Delta\mathbf{k}_f/\mathbf{k}_F)\tan\theta_A - \gamma_2]^2}{\alpha_3^2} + \frac{\gamma_1'^2}{\alpha_1'^2} + \frac{\gamma_2^2}{\alpha_2^2} + \frac{\delta_1'^2}{\beta_1'^2} \\
&\left. + \frac{\delta_1^2}{\beta_1^2} + \frac{\delta_1'^2}{4\sin^2\theta_M \eta_A'^2 + \beta_0^2} + \frac{\delta_2^2}{4\sin^2\theta_A \eta_A'^2 + \beta_3^2} + \frac{\delta_2^2}{\beta_2^2}\right]
\end{aligned}
\tag{1}
$$

where $\gamma_1\gamma_2$ and $\delta_1\delta_2$ are the horizontal and vertical divergences with respect to $\mathbf{k}_I$ and $\mathbf{k}_F$ respectively and γ_1' and δ_1' are the corresponding divergence angles with respect to $\mathbf{k}_I$ in and perpendicular to the monochromator scattering plane. θ_M and θ_A are the monochromator and analyser Bragg angles, η_M, η_M' and η_A, η_A' are the mosaics of the monochromator and analyser in and perpendicular to their corresponding scattering planes. If γ_1' and δ_1' are expressed in terms of γ_1 and δ_1 the equation becomes one of six variables. By substitution of the energy transfer ω and the components of $\Delta\mathbf{Q}$ for $\Delta\mathbf{k}_i$, $\Delta\mathbf{k}_f, \gamma, \delta$ and performing two integrations as described in the Appendix it is possible to arrive at a four-dimensional function $R(\mathbf{Q}+\Delta\mathbf{Q},\omega)$ expressed in terms of $\mathbf{Q}$. $\mathbf{Q}$ may be expressed in terms of an orthogonal set of axes in momentum space such that ΔQ_x lies along $\mathbf{Q}$, ΔQ_y is perpendicular to $\mathbf{Q}$ and lies in the scattering plane and ΔQ_z is perpendicular to the scattering plane. This function is a Gaussian in four dimensions and has the form

$$R(\mathbf{Q}+\Delta\mathbf{Q},\omega)=R_0 \exp -\tfrac{1}{2}\sum_{k=1}^{4}\sum_{l=1}^{4} X_k A_{kl} X_l \qquad (2)$$

where X_1, X_2 and X_3 are ΔQ_x, ΔQ_y and ΔQ_z, the deviations from $\mathbf{Q}$, and X_4 is $\hbar\omega$, the energy transfer. If we equate the exponent in equation (2) to $-0{\cdot}693$ ($=\ln 0{\cdot}5$) we find the locus in $\mathbf{Q}$–ω space for which the resolution function has a value half of that at $\mathbf{X}=0$. This can be seen to be a four-dimensional ellipsoid and this is a convenient form in which to envisage the resolution function of the instrument.

The resolution function

The width of a phonon peak measured by a three-axis spectrometer depends on the shape of the dispersion surface of the specimen under investigation. This four-dimensional surface in $\mathbf{Q}$–ω space has, in the harmonic approximation, zero thickness and the intensity of the detected neutrons for a resolution function centred at some arbitrary point in this space is given by the integral of equation (2) over the surface. This integral may be readily performed for dispersion surfaces described by linear or quadratic equations using a simple method described by Haywood (1970). Where the equation of the dispersion surface is more complex or the surface has a finite thickness a more tedious numerical integration technique may be employed (Samuelson, 1971). In measuring dispersion curves with a three-axis spectrometer, scans are usually performed in which the resolution ellipsoid is passed through the dispersion surface with either $\mathbf{Q}$ or ω kept constant. The intensity of the neutron count rate at any point on this scan, given by the integral of equation (2) over the dispersion surface, rises to a maximum at some point in the scan and produces a peak with finite half width.

The widths of the peaks produced by planar dispersion surfaces are particularly simple to evaluate and this type of surface will be assumed in this paper to demonstrate the effects of increasing the angle between monochromator and specimen planes. This approximation can be used in many experimental situations where the curvature of a dispersion surface is small over the extent of the resolution ellipsoid. It can easily be shown that the full width at half height of a line in this instance is the distance between the points at which the half-value ellipsoid just touches the dispersion surface as it passes through. In this rather simplified analysis it has been assumed that the direction of the scan is coplanar with the normal to the dispersion surface, *i.e.*, that the scan is being made along a symmetry direction. Under these simplifying assumptions the width is found by projecting the four-dimensional ellipsoid on to the plane of ω–$\mathbf{Q}$ space, which contains the normal to the dispersion surface and determining the points at which the line representing the slope of the dispersion curve is tangential to the ellipsoid. This is shown in Fig. 3.

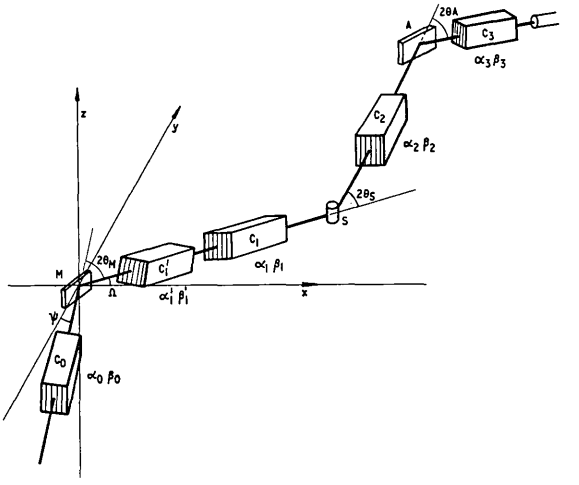

Fig. 1. The experimental arrangement. Collimators C_0 and C_1' are in the monochromator scattering plane and C_1, C_2 and C_3 are in the specimen scattering plane. The divergences α and β are parallel and perpendicular to the scattering plane. M, S and A are the monochromator, specimen and analyser respectively.

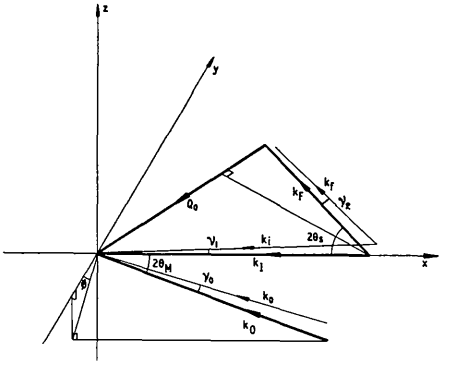

Fig. 2. The reciprocal-space diagram of the experimental arrangement of Fig. 1. The vectors $\mathbf{Q}_0$, $\mathbf{k}_F$ and k_I are coplanar and the plane of $\mathbf{k}_I$ and $\mathbf{k}_0$ is at an angle φ to this plane.

At (*a*) the surface just touches the ellipsoid and we are at a point *a* on the peak; at (*b*) we are centred on the peak and at (*c*) we are at point *c*.

As in the case of the two-axis diffractometer in I the resolution ellipsoid has a principal axis along the *z* direction and this axis is much greater than the two other axes. The effect of increasing the interplanar angle φ is to tilt this ellipsoid so that components from the major axis appear in the projection of the ellipsoid on the *xy* plane.

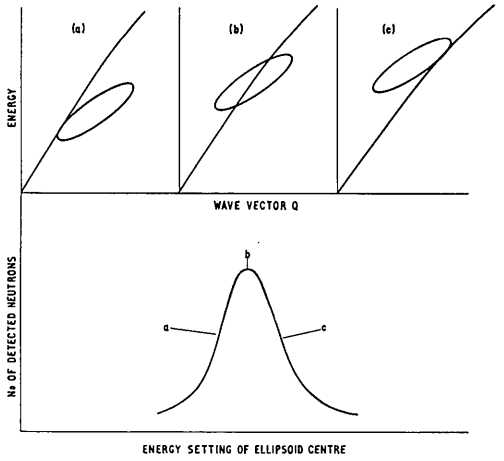

Fig. 3. The position of the half-value resolution ellipsoid at different points in a constant-**Q** scan. In (*a*) the ellipsoid assumed to be moving upwards parallel to the energy axis is just touching the dispersion surface and we are at point *a* in the lower curve. At (*b*) the dispersion surface passes through the centre of the ellipsoid and the detected count rate reaches a maximum. At (*c*) the descending half value is reached.

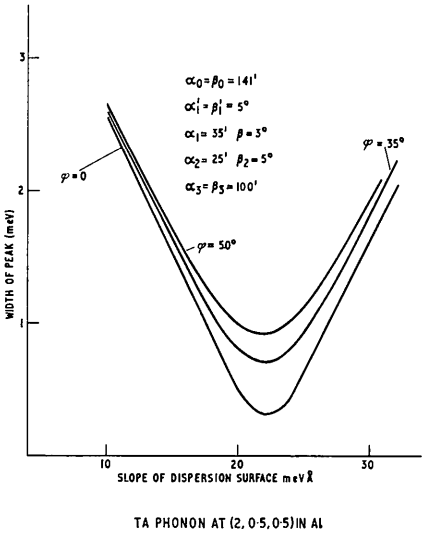

Fig. 4. The measured half width of a three-axis spectrometer as a function of the slope of the dispersion surface under investigation. The experimental parameters are $\alpha_0=\beta_0=140'$, $\alpha_1'=\beta_1'=\beta_2=5°$, $\alpha_1=35'$, $\beta_1=3°$, $\alpha_2=25'$, $\alpha_3=\beta_3=100'$. The value of **Q** was 3·292 Å^{-1}.

The width of the line measured by a three-axis spectrometer is, however, dominated by the extent of the resolution function in the direction of ω. This extent is caused by the spread in energy of the incident and detected beams of neutrons due to the finite collimation at the monochromator and analyser. In practice it is found to be very difficult to reduce this collimation to a point where the energy spread is not the most important factor in the peak width because of the severe loss of intensity incurred. Indeed if it were possible to reduce the energy spread in this way the whole concept of focusing of three-axis spectrometers would be of very much reduced importance.

Calculated results

Focusing in three-axis spectrometry usually consists of matching as closely as possible the slope of the major axis of the resolution function to the slope of the dispersion surface. The effect of varying the slope of the dispersion surface on the width of a typical measured phonon peak is shown in Fig. 4 for various values of the interplanar angle φ of Fig. 2. All of the calculated curves shown in this paper have been calculated on the simplifying assumptions described above, *i.e.*, a plane dispersion surface and constant **Q** scans carried out along symmetry directions. The machine parameters chosen for this resolution function were those used for the measurement of the TA phonon at (2, 0·5, 0·5) in aluminum on the Pluto 3-Axis at A.E.R.E. Harwell and the width of the peak predicted by the calculation is in good agreement with the measured line at the observed slope of 25·3 meV Å. The effect of increasing the interplanar angle φ is to increase the measured line width. At the minimum in the curve the increase is a factor of about two between the conventional spectrometer with $\varphi=0$ and one having $\varphi=35°$. A further increase to $\varphi=50°$ raises the line width to three times that of a normal spectrometer.

Away from the absolute focusing position which occurs at a slope of 22·2 meV Å the resolution suffers less. For example, if the three resolution functions described in Fig. 4 were used to measure the Al phonon at (2, 0·5, 0·5) with energy 25·6 meV and slope 25·3 meV Å, the observed line widths would be in the ratio 1, 1·2, 1·3 for $\varphi=0$, 35, 50°. The projections of the three resolution functions on to the **Q**–ω plane are shown in Fig. 5.

In a constant **Q** scan the resolution ellipsoid, and hence the projected ellipse, is moved vertically up the ω axis. The relative scales of ω and **Q** have been chosen to present the resolution ellipse with a slope of about 50° to the horizontal.

As can be seen, the minor axis of the ellipse increases with φ while the slope and major axis are unaffected. The curves of Fig. 4 can now be explained as follows: near the focusing position, at the minimum of the curves at 22·2 meV Å, the points on the half-value ellipse which are tangential to the dispersion surface

are on the ends of the minor axis of the ellipse. Thus the increase in the length of this axis is reflected directly in increased line width. Away from the focusing position, however, the points on the ellipse tangential to the surface are further from the centre. This means that the line width is much less sensitive to the length of the minor axis of the ellipse and depends much more on the extent of the major axis in the ω direction, which can be seen to be independent of φ in the present case.

The effect of the two collimators C_1 and C_1' is illustrated in Fig. 6. In (*a*) C_1 or C_1' is varied at $\varphi=0$, and in (*b*) and (*c*) C_1' and C_1 are varied at $\varphi=35°$. The machine parameters chosen for these figures were those used on the Pluto three-axis diffractometer for measurement of the 29 meV LA phonon in Al at (0, 1·2, 1·2). Increasing α_1 on the conventional machine ($\varphi=0$) has the effect of increasing the width of the measured lines away from the focusing position. At the focusing position the width increases very slightly mainly owing to the increased width of the projected ellipse in the **Q** direction.

At $\varphi=35°$, if we vary α_1', in the plane of the specimen, and relax α_1, we see from Fig. 6(*b*) that the effect on the line width is mainly confined to the region of high slope of the dispersion curve. The point of minimum width also moves to a lower value of slope as the collimation is relaxed. The effect of relaxing α_1' and varying α_1 in the plane of the monochromator is shown in Fig. 6(*c*). The effect is most marked in the region of low slope of the dispersion curve and it can be seen that the minimum width occurs at a larger value of this slope as α_1 is relaxed.

These results can be explained by considering the effect of each of the collimators. The collimation in the plane of the specimen C_1, with divergences α_1, β_1 improves the definition of the beam falling on the specimen and has little effect on the wavelength spread of the neutrons in that beam. The projections of the half-value ellipsoids for the cases $\alpha_1'=15'$ and $\alpha_1'=60'$ are shown in Fig. 7(*b*) compared with the corresponding projections for $\varphi=0°$ in Fig. 7(*a*). This figure shows that the width of the ellipse is kept almost constant and the length changes by a factor of about two. The effect of variation of the collimation in the plane of the monochromator is shown in Fig. 7(*c*) where the projected ellipse is drawn for $\alpha_1=15$ and $60'$. In this case the width of the ellipse doubles in going from $\alpha_1=15'$ to $\alpha_1=60'$ while the length changes by a factor of only 1·25. Thus in Fig. 6(*b*) as α_1' is varied the slope of the lines of width *vs.* the slope of the dispersion surface will remain relatively constant. The change in position of the focus is a result of the change in slope of the ellipse axes as the collimation is varied.

In Fig. 6(*c*) the result of increasing the width of the projected ellipse while keeping the length relatively constant is shown. In this case the slopes of the lines increase as α_1 is relaxed and the width at the focus remains the same.

An interesting point in these curves is that in each of the cases shown in Fig. 6, the width at the original focus, around 19 meV Å, remains constant. This seems to show that at this value the resolution width is independent of the collimation between monochromator and specimen.

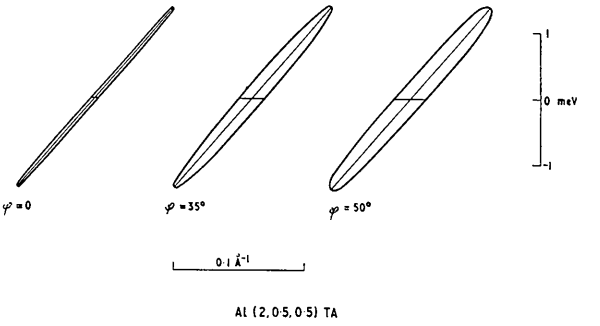

Fig. 5. The projection of the ellipsoids for Fig. 4 onto the **Q**–ω plane. As φ increases the dimensions of the ellipse increase in the **Q** direction while the size in the ω direction remains constant.

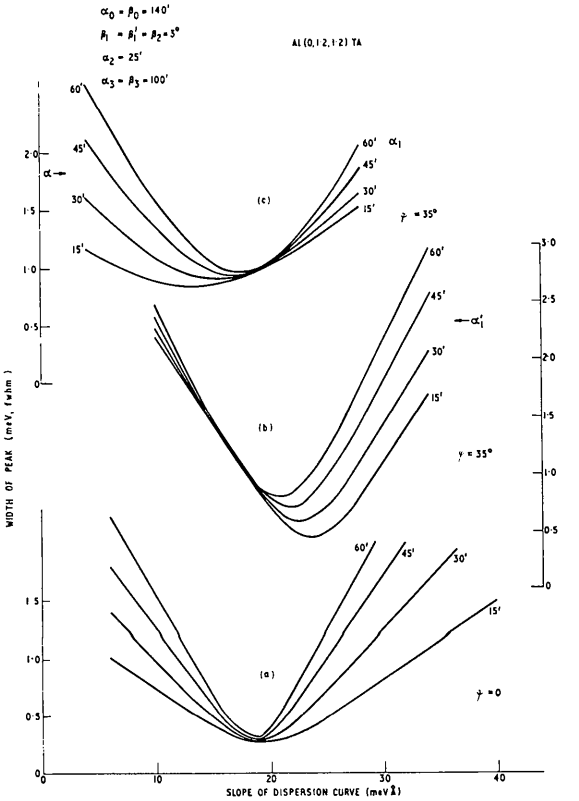

Fig. 6. The effect of variation of α_1' in the monochromator plane, and α in the specimen plane, on the peak widths measured at $\varphi=35°$. The experimental parameters are $\alpha_0=\beta_0=140'$, $\beta_1=\beta_1=\beta_2=3°$, $\alpha_2=25'$, $\alpha_3=\beta_3=100'$. **Q** = 2·634 Å^{-1}. In (*a*) $\varphi=0$ and α_1, and α_1' are equivalent. In (*b*) α_1 is kept at 3° while α_1' is varied and in (*c*) α_1' is kept at 3° while α_1 is varied.

Fig. 8 shows the effect of improvement of the collimation on the resolution of an instrument with $\varphi=35°$. In this figure the solid line shows the resolution expected from a conventional machine with $\varphi=0°$ set up as for the curves of Figs. 4 and 5 but with somewhat tighter collimation to give a better determination of the dispersion curve. The upper dashed curve shows the resolution expected if this collimation is held constant and φ is increased to 35°. The integrated intensity of the measured phonon line remains constant in this case. The lower dotted lines show the effect of reducing the collimation angles α_1, α_1' and α_2 on either side of the specimen. Thus if a phonon or magnon dispersion curve is being measured with a slope of 10 meV Å at this position in $\mathbf{Q}$–ω space the resolution of a machine with $\varphi=0$ and α_1' and α_2 of 26′ can be reproduced by a machine with $\varphi=35°$ and α_1, α_1' and α_2 of 40, 20 and 20′ with a fall in intensity to about 35% of the intensity at $\varphi=0$. The lower dotted curve shows the effect of further reduction of α_1, α_1' and α_2 to 30, 15 and 20′ which results in a fall in intensity to 22%.

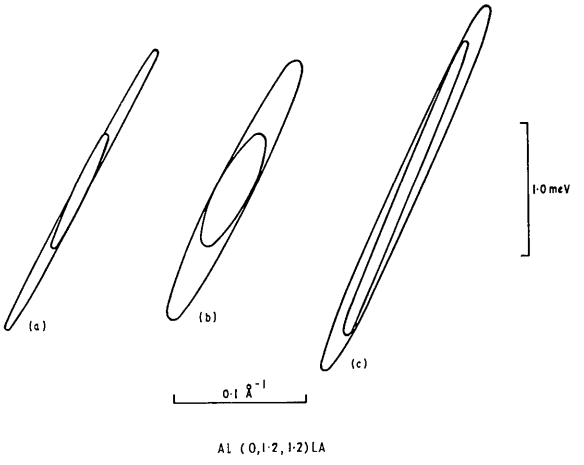

Fig. 7. The projection of the ellipsoids for α_1 or $\alpha_1'=15$ and 60′ for each of the cases in Fig. 6.

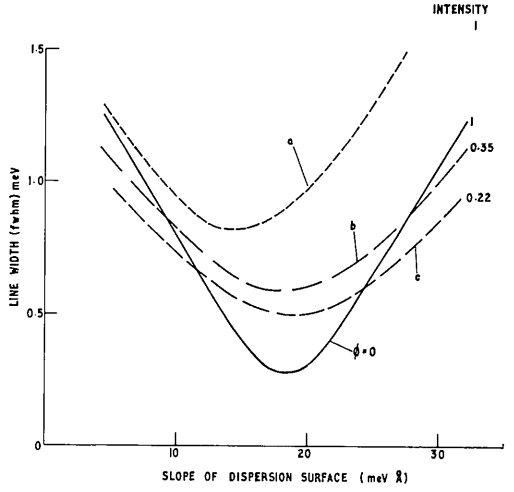

Fig. 8. The effect of collimation on the peak width in a well collimated case. In $\varphi=0$ curve $\alpha_0=\alpha_3=\beta_2=\beta_3=1°$, $\alpha_1=\beta_1=5°$, $\alpha_1'=\alpha_2=26'$, $\beta_1'=3°$, $\beta_0=2°$. $\mathbf{Q}=2{\cdot}634$ Å^{-1}. In (*a*) the parameters are identical but $\varphi=35°$. In (*b*) $\alpha_1=40'$, $\alpha_1'=20'$ and the transmitted intensity is 0·35 times that of (*a*). In (*c*) $\alpha_1=30'$, $\alpha_1'=15'$, $\alpha_2=20'$ and the intensity is 0·22 times that of (*a*).

Discussion of results

The results shown in Figs. 4 and 6 indicate that there is a significant worsening of the resolution of a three-axis spectrometer as the angle between the monochromator and scattering planes is increased. This deterioration is concentrated mainly around the focusing position at the minimum of the curves and is relatively less important away from this setting. In theory, if enough variable experimental parameters are available it is possible to focus a three-axis spectrometer at practically any point in ω–$\mathbf{Q}$ space. In practice, many parameters of the instrument, (such as the monochromator and analyser plane spacings or the various collimation angles), are so difficult to vary during the course of an experiment that they are changed only infrequently and for very special measurements of the highest accuracy. This means that during a normal three-axis spectrometer experiment the machine is optimized for the general region in ω–$\mathbf{Q}$ space in which measurements are to be made and individual phonons or magnons are measured with the best focusing configuration that is available within the overall machine parameters. Thus for the great majority of three-axis experiments optimum focusing is not achieved for each measurement and under these circumstances the increase in line width involved in using an angled hole may not be serious.

The equations given in the Appendix indicate that the total intensity in the measured peak is independent of the degree of focusing and the interplanar angle, and thus once again it is only weak lines, just measurable at the focusing configuration with $\varphi=0$, that would be difficult to measure at other values of φ. It is quite possible to improve the collimation of an instrument to restore the resolution if a sacrifice of intensity can be made as is illustrated by Fig. 8. A reduction of intensity to 30% would be perfectly acceptable if, by such, an experiment could be carried out on a high-flux reactor rather than a conventional medium-flux reactor. A further possibility not considered here is that by curving the monochromator crystal it may be possible to restore both intensity and resolution for certain types of experimental configuration.

Conclusions

The results presented in this paper have shown that a three-axis spectrometer can be conveniently used on an angled reactor channel. The limitations are important only for those experiments where the greatest

intensities and highest resolutions are required. For the great majority of experiments carried out by three-axis spectrometers the configuration suggested here will provide perfectly adequate results.

I would like to thank Dr B. T. M. Willis for several discussions and for help with presentation of the results.

APPENDIX

As in paper I we shall define sets of orthogonal axes $\mathbf{i}_0\mathbf{j}_0\mathbf{l}_0$, $\mathbf{i}_1'\mathbf{j}_1'\mathbf{l}_1'$, $\mathbf{i}_2\mathbf{j}_2\mathbf{l}_2$ such that $\mathbf{i}_0$, $\mathbf{i}_1'$ and $\mathbf{i}_2$ are parallel to $-\mathbf{Q}_0$, $\mathbf{k}_I$ and $\mathbf{k}_F$ and $\mathbf{l}_0$, $\mathbf{l}_1$ and $\mathbf{l}_2$ are vertical.

If $\Delta\mathbf{k}_i$ has components $x_1'y_1'z_1'$ along $\mathbf{i}_1'\mathbf{j}_1'$ and $\mathbf{l}_1'$ and $\Delta\mathbf{k}_f$ has components $x_2y_2z_2$ along $\mathbf{i}_2\mathbf{j}_2$ and $\mathbf{l}_2$ we find

$$\Delta\mathbf{k}_i=(x_1'\beta+y_1'\alpha)\mathbf{i}_0+(y_1'\beta-x_1'\alpha)\mathbf{j}_0+z_1'\mathbf{l}_0' \tag{A1}$$

$$\Delta\mathbf{k}_f=(x_2\xi+y_2\eta)\mathbf{l}_0+(y_2\xi-x_2\eta)\mathbf{j}_0+z_2\mathbf{l}_0 \tag{A2}$$

where α and β are $\sin\chi$ and $\cos\chi$ and η and ξ are $\sin(2\theta+\chi)$ and $\cos(2\theta+\chi)$ respectively; χ is the angle between $\mathbf{k}_i$ and $-\mathbf{Q}$.

From equations (A1) and (A2) we then have

$$\left.\begin{aligned}\Delta Q_x&=x_2\xi+y_2\eta-x_1'\beta-y_1'\alpha\\ \Delta Q_y&=-x_2\eta+y_2\xi+x_1'\alpha-y_1'\beta\\ \Delta Q_z&=z_2-z_1\,.\end{aligned}\right\} \tag{A3}$$

We also have the relationship

$$\hbar\omega=\frac{h^2}{2m}(k_i^2-k_f^2)$$

from which we find

$$\frac{\hbar}{m}\,x_2k_F=\frac{\hbar}{m}\,x_1'k_I-\Delta\omega\,,$$

giving

$$\frac{m\Delta\omega}{\hbar k_F}=\Omega=\frac{k_I}{k_F}\,x_1'-x_2\,. \tag{A4}$$

We may now define new coordinates $\mathbf{i}_1\mathbf{j}_1\mathbf{k}_1$ by rotation of the $\mathbf{i}_1'\mathbf{j}_1'\mathbf{k}_1'$ triad about $\mathbf{i}_1'$ through an angle φ, giving rise to new variables $x_1y_1z_1$ related to $x_1'y_1'z_1'$ by the relationships

$$\begin{aligned}x_1'&=x_1\\ y_1'&=y_1\cos\varphi+z_1\sin\varphi\\ z_1'&=z_1\cos\varphi-y_1\sin\varphi\,.\end{aligned}$$

Substituting into (*A*3) we find

$$\begin{aligned}\Delta Q_x&=x_2\xi+y_2\eta-\alpha_1\beta-y_1\alpha\delta-z_1\alpha\gamma\\ \Delta Q_y&=-x_2\eta+y_2\xi+x_1\alpha-y_1\beta-z_1\beta\gamma\\ \Delta Q_z&=z_2-z_1\delta+y_1\gamma\end{aligned}$$

where $\gamma=\sin\varphi$ and $\delta=\cos\varphi$; thus

$$y_2=\frac{\Delta Q_x}{B_6}-\frac{\alpha}{\beta}\,\frac{\Delta Q_y}{B_6}+\Omega B_1-Sx_1 \tag{A5}$$

$$z_2=\frac{\delta\xi}{\beta\gamma}\,\frac{\Delta Q_x}{B_6}-\frac{\delta}{\beta\gamma}\left(1+\frac{\xi\alpha}{\beta B_6}\right)\Delta Q_y+\frac{\delta}{\beta}(\eta+\xi B_1)\Omega$$

$$+\frac{x_1\delta}{\beta\gamma}(S\xi+\alpha-p\eta)-\frac{y_1}{\gamma} \tag{A6}$$

$$z_1=\frac{z_2}{\delta}-\frac{\Delta Q_z}{\delta}+\frac{y_1\gamma}{\delta} \tag{A7}$$

$$x_2=px_1-\Omega \tag{A8}$$

where

$$B_6=\eta-\frac{\xi\alpha}{\beta}=\frac{\sin 2\theta}{\cos\varphi}$$

$$B_1=\left(\xi+\frac{\alpha\eta}{\beta}\right)\frac{1}{B_6}=\cot 2\theta$$

$$p=k_I/k_F$$

and

$$S=p\left(\xi+\frac{\alpha\eta}{\beta}\right)-\frac{1}{B_6}=p\cot 2\theta-\frac{\cos\varphi}{\cos\chi\sin 2\theta}\,.$$

We must also specify two new variables y_3 and z_3 for the collimator C_1, equivalent to the variables y_1 and z_1 of CN

$$y_3=(\cos 2\theta-p)/\sin 2\theta\;x+\Delta Q_x/\sin 2\theta-\eta\Delta Q_y/\sin 2\theta$$
$$+\Omega/\sin 2\theta$$
$$z_3=z_2-\Delta Q_z\,.$$

The transmission of the system is now, from equation (1) and CN equation (41)

$$T\propto J\iint\exp-\tfrac{1}{2}[(ax_1+by_1)^2+(cx_1+dy_1)^2(ex_2+fy_2)^2$$
$$+(gx_2+hy_2)^2+jy_1^2+qy_2^2+lz_1^2+mz_2^2+j_1y_3^2+l_1z_3^2]\mathrm{d}x_1\mathrm{d}y_1$$

where

$$a=\frac{\tan\theta_M}{\eta_Mk_I}\qquad b=\frac{1}{\eta_Mk_I}\,,\qquad c=\frac{\tan\theta_A}{\eta_Ak_F}\,,$$

$$d=\frac{-1}{\eta_Ak_F}\,,\qquad e=\frac{2\tan\theta_M}{\alpha_0k_I}\qquad f=\frac{1}{\alpha_0k_I}\,,$$

$$g=\frac{2\tan\theta_A}{\alpha_3k_F}\,,\qquad h=\frac{-1}{\alpha_3k_F}\,,\qquad j=\frac{1}{\alpha_1'k_I}\,,$$

$$q=\frac{1}{\alpha_2k_F}\,,\qquad l=\frac{1}{(4\sin^2\theta_M\eta_M'^2+\beta_0^2)}\,k_I^2+\frac{1}{\beta_1'^2k_I^2}$$

$$m=\frac{1}{(4\sin^2\theta_A\eta_A'+\beta_3^2)}\,k_F^2+\frac{1}{\beta_2^2k_F^2}\,,$$

$$l_1=\frac{1}{\beta_1^2k_I^2}\,,\qquad j_1=\frac{1}{\alpha_1^2k_I}\,.$$

J is the Jacobian of the transformation from $x_2y_2z_1z_2$ to $\Delta Q_x\Delta Q_y\Delta Q_z$ and Ω using equations (*A*5) to (*A*8),

the $\alpha_n S$ and $\beta_n S$ are the horizontal and vertical divergences of collimator C_n and η and η' are the mosaic spreads of the crystals in and perpendicular to their respective scattering planes.

Then defining

$$L_1 = \frac{B_2}{B_6^2} + D_0 A_1^2 + \frac{j_1 \xi}{\beta B_6}$$

$$L_2 = \frac{\alpha^2}{\beta^2}\frac{B_2}{B_6^2} + D_0 A_2^2 - j\frac{\eta}{1\beta B_6}$$

$$L_4 = B_4 + B_1^2 B_2 + D_0 A_3^2 + \frac{j_1}{\beta B_6} - 2B_5 B_1$$

$$L_5 = \frac{-B_2\alpha}{\beta B_6^2} + D_0 A_1 A_2 - j_1 \frac{\eta\xi}{B_6^2\beta^2}$$

$$L_7 = \frac{B_2 B_1}{B_6} - \frac{B_5}{B_6} + D_0 A_1 A_3 + \frac{j_1\xi}{\beta^2 B_6^2}$$

$$L_9 = \frac{-B_2 B_1 \alpha}{\beta B_6} + D_0 A_2 A_3 - j_1 \frac{\eta}{\beta^2 B_6^2}$$

$$A_3 = (\eta + \xi B_1)/\beta\gamma, \quad A_2 = \left(1 + \frac{\xi\alpha}{\beta B_6}\right)\frac{1}{\beta\gamma}, \quad A_1 = \frac{\xi}{\beta\gamma B_6}$$

$$B_2 = f^2 + g^2 + h^2, \quad B_4 = e^2 + g^2 \quad B_5 = ef + gh$$

$$D_0 = l + (l_1 + m)\delta^2$$

$$J_4 = \frac{B_2 S + B_5 p}{B_6} + D_1 A_1 + J_1 \frac{C\xi}{\beta B_6}$$

$$J_5 = \frac{-(B_2 s + B_5 p)}{B_6}\frac{\alpha}{\beta} + D_1 A_2 - J_1 \frac{C\eta}{\beta B_6}$$

$$J_6 = (B_2 s + B_5 p)B_1 - B_4 p - B_5 s + D_1 A_3 + j_1 C/\beta B_6$$

$$F = a^2 + c^2 + p^2 B_4 + s^2 B_2 + 2ps B_5 + lr^2 + (m + l_1)\omega^2 + j_1 C^2$$

$$C = (B_1 B_6 \beta - p)/B_6\beta, \quad w = \frac{\delta}{\beta\gamma}(s + \alpha - p\eta) = r\delta$$

$$D_1 = lr + (m + l_1)\omega\delta$$

$$H = ab + cd + lrt - (m\omega + l_1\omega)/\gamma$$

$$M_1 = A_1\delta D_2 - \frac{J_4 H}{F}, \quad M_2 = \frac{-A_2\delta D_2}{\gamma} - \frac{J_5 H}{F}$$

$$M_3 = \frac{-m}{\gamma} - \frac{mw}{F}H, \quad M_4 = \frac{-A_3}{\gamma} - \frac{J_6 H}{F},$$

we finally arrive at the result that

$$T = \frac{1}{\beta B_6}\frac{1}{\gamma}\left(\frac{\pi^3}{8(FG - H^2)}\right)^{1/2} \times \exp - \left(\tfrac{1}{2}\sum_{l=1}^{4}\sum_{j=1}^{4} X_l R_{lj} X_j\right)$$

where X_{1-3} are $\Delta Q_x \Delta Q_y \Delta Q_z$, X_4 is Ω, and

$$G = b^2 + d^2 + j + \frac{l\delta^2}{\gamma^2} + (m + l_1)/\gamma^2 P = FG - H^2$$

$$R_{11} = L_1 - \frac{J_4^2}{F} - \frac{M_1^2}{P}, \quad R_{22} = L_2 - \frac{J_5^2}{F} - \frac{M_2^2}{P}$$

$$R_{33} = m - \frac{m^2 w^2}{F} - \frac{M_3^2}{P}, \quad R_{44} = L_4 - \frac{J_6^2}{F} - \frac{M_4^2}{P}$$

$$R_{12} = L_5 - \frac{J_4 J_5}{F} - \frac{M_1 M_2}{P}$$

$$R_{13} = m\delta A_1 - \frac{J_4 mw}{F} - \frac{M_1 M_3}{P}$$

$$R_{14} = L_7 - \frac{J_4 J_6}{F} - \frac{M_1 M_4}{P}$$

$$R_{23} = m\delta A_2 - \frac{J_5 mw}{F} - \frac{M_2 M_3}{P}$$

$$R_{24} = L_9 - \frac{J_5 J_6}{F} - \frac{M_2 M_4}{P}$$

$$R_{34} = m\delta A_3 - \frac{mwJ_6}{F} - \frac{M_3 M_4}{P}.$$

References

BJERRUM MØLLER, H. & NIELSON, M. (1970). *Instrumentation for Neutron Inelastic Scattering Research*, pp. 49–76. Vienna: I.A.E.A.

COLLINS, M. F. (1963). *Brit. J. Appl. Phys.* **14**, 805.

COOPER, M. J. & NATHANS, R. (1967). *Acta Cryst.* **23**, 357–367.

CHESSER, N. J. & AXE, J. D. (1973). *Acta Cryst.* A**29**, 160–169.

HAYWOOD, B. C. G. (1970). *Acta Cryst.* A**27**, 408–410.

HAYWOOD, B. C. G. (1974). *Acta Cryst.* A**30**, 448–453.

SAMUELSON, E. J. (1971). *Structural Phase Transitions and Soft Modes*. Edited by E. J. SAMUELSON, E. ANDERSEN & J. FEDER, pp. 189–215. Oslo Universitetsforlaget.